Available online at www.sciencedirect.com

SciVerse ScienceDirect

Procedia Environmental Sciences 13 (2012) 742 – 754

Procedia Environmental Sciences

The 18th Biennial Conference of International Society for Ecological Modelling

Modeling gross primary production of two steppes in Northern China using MODIS time series and climate data

J.F. Liu[a,b*], S.P. Chen[b], X.G. Han[b]

[a]*Key Laboratory of Tree Breeding and Cultivation of State Forestry Administration ,Research Institute of Forestry, Chinese Academy of Forestry, Beijing 100091, China*

[b]*State Key Laboratory of Vegetation and Environmental Change, Institute of Botany, Chinese Academy of Science, No.20 Nanxincun, Xiangshan, Beijing 100093, China*

Abstract

Terrestrial carbon cycle plays an important role in global climate change. As a key component of terrestrial carbon cycle, gross primary production (GPP) is a major determinant of the exchange of carbon between the atmosphere and terrestrial ecosystems. With rapid advancement of remote-sensing technology, it has become a common practice to utilize parameters derived from remote-sensing data to estimate GPP at a regional or global scale. In this study, a satellite-driven model, Vegetation Photosynthesis Model (VPM) was introduced to estimate GPP of two steppes, Xilinhot (XH, 43.5544°N, 116.6714°E) and Duolun (DL, 42.0467°N, 116.2836°E), at Inner Mongolia in Northern China, by integrating moderate resolution imaging spectral radiometer (MODIS) and meteorological measurements at the two flux towers. As defined by the input variables of VPM, two improved vegetation indices (enhanced vegetation index (EVI) and land surface water index (LSWI)) derived from the standard data product MOD09A1 of MODIS, air temperature and photosynthetic active radiation at the flux towers, were included for the model calculating. Canopy-level maximum light use efficiency, a key parameter for VPM, was estimated by using the observed CO_2 flux data and photosynthetic active radiation (PAR). Observed GPP derived from flux data were then used to critically evaluate the performance of the model. The results indicate that the seasonal dynamics of GPP predicted by the VPM model agreed well with measured GPP by the flux towers. The determination coefficient (R^2) of predicted GPP with measured GPP was 0.86 and 0.79 in 2006, 0.66 and 0.76 in 2007 for DL and XH, respectively. Further, time-series data for the EVI have a stronger linear relationship with the GPP than those for the Normalized Difference Vegetation Index. Results of this study demonstrate that the satellite-driven VPM has been potential for estimating site-level or regional grassland GPP, and might be an effective tool for scaling-up carbon fluxes.

* Corresponding author. Tel.: +86-10-62889054; fax: +86-10-62872015.
E-mail address: Liujf@caf.ac.cn / Liujf2000cn@163.com.

1878-0296 © 2011 Published by Elsevier B.V. Selection and/or peer-review under responsibility of School of Environment, Beijing Normal University. Open access under CC BY-NC-ND license. doi:10.1016/j.proenv.2012.01.068

Key words: Gross primary production; steppe; vegetation photosynthesis model; northern China

1. Introduction

The gross primary production of vegetation is a key component of land-atmosphere interaction, determines the strength of the carbon sink of terrestrial ecosystems. Eurasian grassland regions are the largest and most characteristic in the world, although their vegetation exhibits regional characteristics. The typical Eurasian steppe is widely distributed in the eastern Eurasian steppe zone, which has a total area of ~4.1 ×107 hm^2, half of which in China. Within China, typical steppes are distributed throughout the Northeastern Plain and eastern Inner Mongolia Plateau, with about 10.5% of the national grassland area under a temperate, semi-arid climate [1, 2]. The climate in this area has been displaying a warming trend, accompanied by a clear increase in air temperature during winter and serious drought in spring. And this pattern has potential serious consequences for primary production.

Field-based continues measurements from fixed platforms, such as eddy covariance (EC) flux towers, is one of the most useful micrometeorological methods for estimating the carbon exchange between terrestrial ecosystems and the atmosphere [3]. However, EC measurements only represent the fluxes within its own footprint, which can be up to several square kilometers over a heterogeneous land surface [4]. It remains a challenging task to extrapolate EC measurements from sparsely distributed flux towers to meaningful vegetation parameters at the regional scale.

Satellite remote-sensing data with various temporal-spatial resolutions have greatly enhanced the global and regional-scale observations of vegetation dynamics, and has played an increasing role in scaling EC measurements to large areas [5-7]. An integrated method of remote-sensing data and flux measurements could be extremely helpful for improving spatially extended estimates of vegetation production with high accuracy. The Vegetation Photosynthesis Model (VPM), a remote sensing-based model that recently developed by Xiao *et al* [8,9], has successfully demonstrated its great potential for scaling-up GPP from flux tower sites to the regional scale by integrating remote-sensing data and flux measurements, such as in forests [8-12], grasslands [3, 13-15], and croplands [14,16]. However, the application and comparison of VPM to typical steppes over various climates are still scarcely [14, 15]. Liu *et al* [15] also found it was difficult for the water scalar, which derived from the LSWI (MODIS), in the VPM model to reflect grassland ecosystem soil water status, especially for the dry year, whereas soil water content was a dominant factor for ecosystem primary production. The goal of this study was to test whether VPM has the ability to describe the characteristics of GPP in two typical steppes, located at Inner Mongolia, with various climates and vegetation species composition. Specifically, the objectives of this study were the following: (1) to study the characteristics of GPP in the two steppes; (2) to compare the relationship between the vegetation indices and GPP; and (3) to evaluate the GPP predicted by VPM with the EC measured GPP. Finally, the potential of Satellite remote sensing for studying and monitoring vegetation and carbon fluxes in typical steppes of China will be explored.

2. Materials and methods

2.1. Brief description of the study sites

This study was conducted at eastern Inner Mongolia, China, that typifies with the continental, semi-arid monsoon region of eastern Eurasia. The growing season usually starts in late April and ends in late September.

Duolun (ab.DL, 42.0467°N, 116.2836°E, 1350 m asl) is located within a typical semi-arid, agro-pastoral transit zone between the North China Plain and Inner Mongolia. According to the long-term climate data (1994–2004) from a meteorological station in Duolun, the mean monthly air temperatures ranged from 15.9 ℃ in January to 19.9 ℃ in July and the annual mean temperature was 3.3 ℃. Mean annual precipitation was 399 mm, with the maximum monthly value occurring in July or August. The average growing season was about 150 days. The dominant soil type was chestnut soil. The type of vegetation cover in this study site is the typical steppe, which was the primary native vegetation type of this arid region and was dominated by *Stipa krylovii*, *Agropyron cristatum*, *Artemisia frigida*, *Cleistogenes squarrosa* and *Leymus chinensis*. Our study site was located at the permanent study plot (>50 ha) fenced to exclude grazing by the Duolun Restoration Ecology Research Station in 2001[17].

Xilinhot (ab. XH, 43.5544°N, 116.6714°E, 1250m asl) is located in the typical steppe zone of the Inner Mongolia Plateau. In contrast with the Duolun region, livestock grazing is the primary land use type in the Xilinhot region, with all the steppes heavily degraded due to overgrazing. The average annual temperature of Xilinhot region was 2.0 ℃, with January as the coldest month (-22.3 ℃) and July as the hottest month (18.8 ℃). Annual precipitation was 350 mm and 80% of this occurred between June and September [2]. Chestnut and dark chestnut soils were the zonal soil types found in this region [18]. This degraded steppe site had been fenced since May of 2005, and with the vegetation dominated by *Stipa grandis*, *Artemisia frigida*. More details of the two sites can be seen in [19], including eddy covariance installation equipments.

2.2. Estimation of gross primary production from flux data

The eddy covariance technique greatly facilitates the estimates of *GPP* over various ecosystems. At our study sites, the daily flux data of net ecosystem CO_2 exchange (*NEE*), ecosystem respiration (*Re*), and GPP were generated from the half-hourly flux data collected during the total growing seasons of 2006 and 2007 (April to October). Webb-Pearman-Leuning (*WPL*) corrections and three-dimension coordinate rotations were firstly made to correct for the density and tilt effects [20, 21]. Then anomalous or spurious values caused by sensor malfunction and rain events were removed from the datasets. *NEE* data of the friction velocity (U^*) $\leqslant$ 0.15 m s^{-1} during nighttime were also rejected. Gap filling of missing data were achieved using different strategies. For gaps $\leqslant$ 2 hours, the missing *NEE* data were linearly interpolated. For large gaps (>2 hours), the daytime NEE data (NEE_{day}) (incident solar radiation > 0.5 W m^{-2}) were estimated as a function of *PAR* with the Michaelis – Menten equation [22] on a monthly basis:

$$NEE_{day} = (\alpha \times \beta \times PAR) / (\alpha \times PAR + \beta) - Re \quad (1)$$

where α is the apparent quantum yield or initial slope of the light response curve, β is the value of the *NEE* at light saturation, and *Re* is the respiration term. The nighttime *NEE* data gaps were filled by using the empirical relationships between ecosystem respiration and surface air temperature under high turbulence:

$$NEE_{night} = R_{ref,10} \times Q_{10}^{(T-10)/T} \quad (2)$$

Where NEE_{night} is nocturnal ecosystem respiration, $R_{ref,10}$ is ecosystem respiration on 10℃ reference temperature, Q_{10} is the change in the rate of respiration with a 10℃ change of temperature, T is air temperature near the ground. The resultant regression equation was used to predict ecosystem respiration during daytime in combination with measured surface air temperature. *GPP* was derived by subtracting the daytime ecosystem respiration (R_{eco}) from the corresponding daytime *NEE*. Daily climate and *GPP*

data were aggregated to 8-day intervals to be consistent with the MODIS 8-day composites, including 8-day sums of *PAR* and 8-day means of daytime air temperature.

2.3 8-Day composite images from MODIS sensor

The MODIS sensor acquires images in 36 spectral bands where seven bands are designed for the study of vegetation and land surfaces: blue (459–479 nm), green (545–565 nm), red (620–670 nm), NIR (841–875 nm, 1230–1250 nm), and SWIR (1628–1652 nm, 2105–2155 nm). The MODIS Land Science Team provides several data products derived from MODIS observations to the public, including the 8-day composite Land Surface Reflectance (MOD09A1). The MOD09A1 datasets include seven spectral bands mentioned above at a spatial resolution of 500-m, and have been corrected for the effects of atmospheric gases, aerosols, and thin cirrus clouds.

In this study, we downloaded images for January 2006 to December 2007 and extracted land surface reflectance data of MODIS pixels, based on the geo-location information (latitude and longitude) of these two eddy covariance flux sites in Xilinhot and Duolun station. Time series MODIS data from one MODIS pixel, 3×3 MODIS pixels and 5×5 MODIS pixels for VI in the VPM model were extracted but no significant difference was found after comparisons, so in this paper we only report the data from one pixel (500m×500m). Land surface reflectance values from four spectral bands (blue, red, NIR (841–875 nm) and SWIR (1628–1652 nm)) were used to calculate three vegetation indices: the Normalized Difference Vegetation Index (*NDVI*) [23], the Enhanced Vegetation Index (*EVI*) [24], and the Land Surface Water Index (*LSWI*) [8]:

$$NDVI = (\rho_{nir} - \rho_{red}) / (\rho_{nir} + \rho_{red}) \quad (3)$$

$$EVI = 2.5 \times (\rho_{nir} - \rho_{red}) / (\rho_{nir} + (6 \times \rho_{red} - 7.5 \times \rho_{blue}) + 1) \quad (4)$$

$$LSWI = (\rho_{nir} - \rho_{swir}) / (\rho_{nir} + \rho_{swir}) \quad (5)$$

where ρ_{nir}, ρ_{red}, ρ_{swir}, ρ_{blue} are reflectances of the near infrared, red, shortwave infrared and blue bands, respectively.

2.3. The Vegetation Photosynthesis Model (VPM)

2.3.1. Model structure

The VPM model is based on the concept that leaves and canopy are composed of photosynthetic active vegetation (mostly chlorophyll) and non-photosynthetic vegetation (*NPV*). Thus the Fraction of Absorbed Photosynthetic Active Radiation (*FPAR*) is partitioned into the fraction absorbed by chlorophyll ($FPAR_{chl}$) and the fraction absorbed by NPV ($FPAR_{NPV}$). Note that only the $FPAR_{chl}$ is used for photosynthesis. *GPP* can be described by:

$$GPP = \varepsilon_g \times FPARchl \times PAR \quad (6)$$

$$FPAR_{chl} = k \times EVI \quad (7)$$

$$\varepsilon_g = \varepsilon_0 \times T_{scalar} \times W_{scalar} \times P_{scalar} \quad (8)$$

where ε_g is the light use efficiency (g C mol^{-1} *PAR*), *PAR* is the Photosynthetic Active Radiation (mol m^{-2} s^{-1}, photosynthetic photon flux density, PPFD), $FPAR_{chl}$ is the fraction of *PAR* absorbed by chlorophyll; *EVI* is Enhanced Vegetation Index, k is the coefficient in the *EVI*-$FPAR_{chl}$ linear function; ε_0 is the maximum light use efficiency (g C mol^{-1} *PAR*), and T_{scalar}, W_{scalar}, and P_{scalar} are the down regulation scalars for the effects of temperature, water, and leaf phenology on the light use efficiency of vegetation, respectively.

The VPM model uses *EVI* to estimated $FPAR_{chl}$, with the coefficient *k* being set to 1 [8].The parameter ε_g is estimated as a function of the maximum light use efficiency (ε_0) and down-regulation factors ranging between 0 and 1:

$$T_{scalar} = (T - T_{min})(T - T_{max}) / [(T - T_{min})(T - T_{max}) - (T - T_{opt})^2] \quad (9)$$

$$W_{scalar} = (1+LSWI) / (1+LSWI_{max}) \quad (10)$$

$$P_{scalar} = (1 + LSWI) / 2 \quad (11)$$

where T_{scalar} accounts for effects of temperature on canopy photosynthesis, using the equation developed for the Terrestrial Ecosystem Model [25]; T_{min}, T_{max}, and T_{opt} are the minimum, maximum and optimum temperature for photosynthetic activities, respectively; W_{scalar} represents the effect of water on plant photosynthesis with $LSWI_{max}$ being the maximum *LSWI* value within the plant-growing season for each site (or pixel); and P_{scalar} accounts for effects of leaf age on canopy photosynthesis, using *LSWI* to identify the green-up and senescence phases. For deciduous vegetation, P_{scalar} is computed as a linear function of *LSWI* from bud burst to leaf full expansion, and after that it is set to 1.

2.3.2. Estimation of model parameters

In this study, the maximum light use efficiency (ε_0) can be obtained from the canopy-scale quantum yield (α), which represents the initial slope of the relationship between the *NEE* of CO_2 and the incident photosynthetic photon flux density. It is a parameter used by many biogeochemical carbon cycling models to translate remotely sensed radiation measurements to an estimation of carbon uptake [26]. The value of α can be obtained from the analysis of the *NEE* of CO_2 and incident *PAR* measured from the CO_2 eddy flux tower. In this study, we directly used the value of α derived from the rectangular hyperbola which used for daytime *NEE* gap filling on a monthly basis. The seasonal and inter-annual evolution of α is shown in figure 3. The maximum of monthly average α generally appeared in June and July with values in the range 0.17–0.26 g C mol^{-1} *PAR*. These values are well within the range of reported values for other grass canopies [14].

In the calculation of T_{scalar}, T_{min}, T_{opt} and T_{max} were set as 0, 20 and 35 ^oC for DL site, -2, 20 and 35 ^oC for XH site, respectively, based on the relationship between temperature and photosynthesis. To compute W_{scalar}, we used the maximum *LSWI* ($LSWI_{max}$) value within the two growing seasons for each site. *LSWI* values in winter are often affected by snow cover in winter and not used in the VPM model. For grassland always has new leaves emerging during the plant-growing season, P_{scalar} was set to 1 directly in this study [8].

2.3.3. Statistical analysis

Model accuracy was evaluated using several different statistical indices. The first index used was the relative error (*RE*) between predicted and observed data:

$$RE = [(O-P) / O] \times 100\% \quad (12)$$

where O is the sum of observed data, and P is the sum of predicted data. Small values of RE indicate better model predictions. Another was the index of agreement (IA) [27]. This index determines the degree to which magnitudes and signs of the observed value about the mean of observed values ($\bar{O}$) are related to the predicted deviation about the mean predicted value, and allows for sensitivity toward differences in observed and predicted values as well as proportionality changes.

$$IA = 1 - [\Sigma(P_i - O_i)^2] / [\Sigma(|P_i - \bar{O}| + |O_i - \bar{O}|)^2] \quad (13)$$

As a non-dimensional measure, IA is bounded below by 0 and above by 1. When two data sets are in perfect agreement, IA equals 1.Simple linear regression between simulations and observations were also used to evaluate model performance, and carried out with SPSS v16.0.

3. Result

3.1. Seasonal dynamics of NEE and GPP

The *NEE* and *GPP* time series in 2006 and 2007 for the two steppe ecosystems had a distinct seasonal cycle (Fig.1). The seasonal dynamics of *GPP* can be explained in part by the seasonal dynamics of air temperature and photosynthetic active radiation (*PAR*) (Fig.2). During the earlier (April) and later (October) period of the growing seasons, *GPP* values were near zero and *NEE* were mostly dominated by ecosystem respiration (*Re*), for low air temperature inhibit photosynthetic activities of the steppe ecosystems. From the start of April as air temperature increased and soil thawed, as well as photosynthetic active radiation intensified, the vegetation began to grow and gross primary production gradually increased, and reached its peak during the July or August. Then *GPP* declined gradually as temperature descended and vegetation started to wither. Photosynthetic capability of the two steppes differed in the two growing seasons, especially for DL in 2007. The peak and total *GPP* during the growing season (from April to October) for DL in 2006 and 2007 were 34.2 g C m^{-2} $8day^{-1}$ and 338.8 g C m^{-2}, 18.9 g C m^{-2} $8day^{-1}$ and 230.1 g C m^{-2}, respectively. The corresponding values for the northern steppe, XH, were 24.8 g C m^{-2} 8 day^{-1} and 313.9 g C m^{-2}, 32.4 g C m^{-2} $8day^{-1}$ and 366.7 g C m^{-2}, respectively.

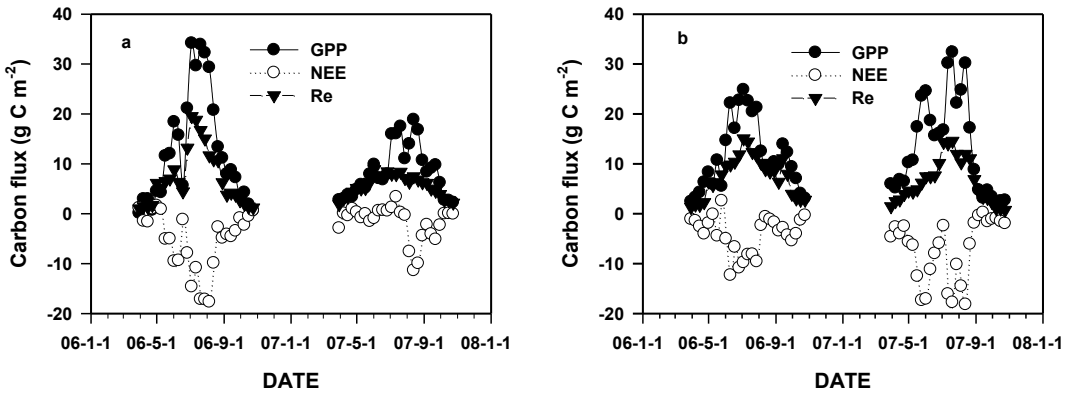

Fig. 1 Seasonal dynamic of *GPP*, *Re* and *NEE* at the two steppes (a: DL; b: XH) in 2006 and 2007.

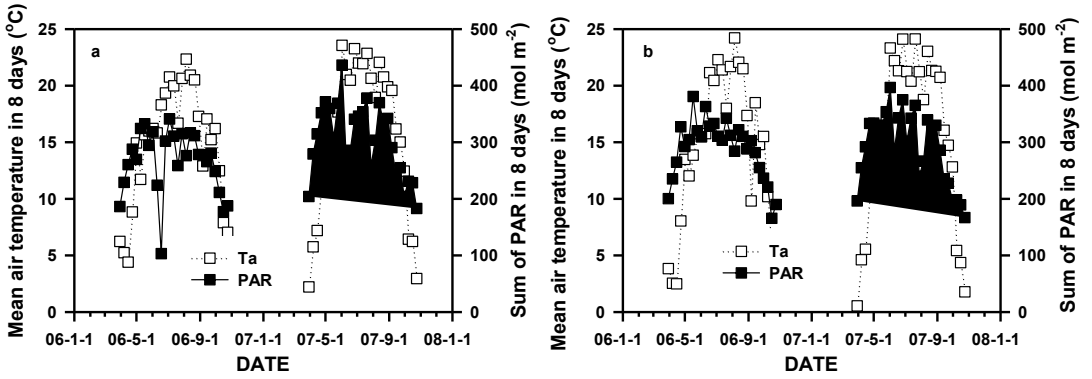

Fig. 2 Seasonal dynamic of air temperature and photosynthetic active radiation at the two steppes (DL: a; XH: b) in 2006 and 2007.

3.2. Seasonal dynamics of vegetation indices

Fig.3 exhibits the seasonal dynamics of *EVI*, *NDVI* and *LSWI* during 2006–2007 at the two steppes ecosystems in Inner Mongolia, north China. The *EVI* and *NDVI* curves were derived from the standard 8-day MOD09A1 surface reflectance products and mimicked the development and senescence of vegetation well. *EVI* and *NDVI* began to increase in spring and reached their maximum values during July to August, then started to decline and remained low in winter. In winter, *EVI* and *NDVI* values were both low. As the *LSWI* curve had reached the highest values at the same time. This was because snow cover and icy soil in winter changed the surface reflectance. There was a distinct difference, however, in the *VI-GPP* relationships between *EVI* and *NDVI*. In both steppes, *EVI* had a stronger linear relationship with *GPP* than *NDVI* (Fig. 7). There were strong linear correlations between the two vegetation indices and *GPP* for DL: $R^2 = 0.749$ for *NDVI*, and $R^2 = 0.802$ for *EVI*. For the degraded grassland site XH, because of low vegetation coverage, the linear relationship was not as good as DL; however, *EVI* correlated well with *GPP* having an $R^2 = 0.643$, while *NDVI* had an $R^2 = 0.570$. The results were all significant at 5% level.

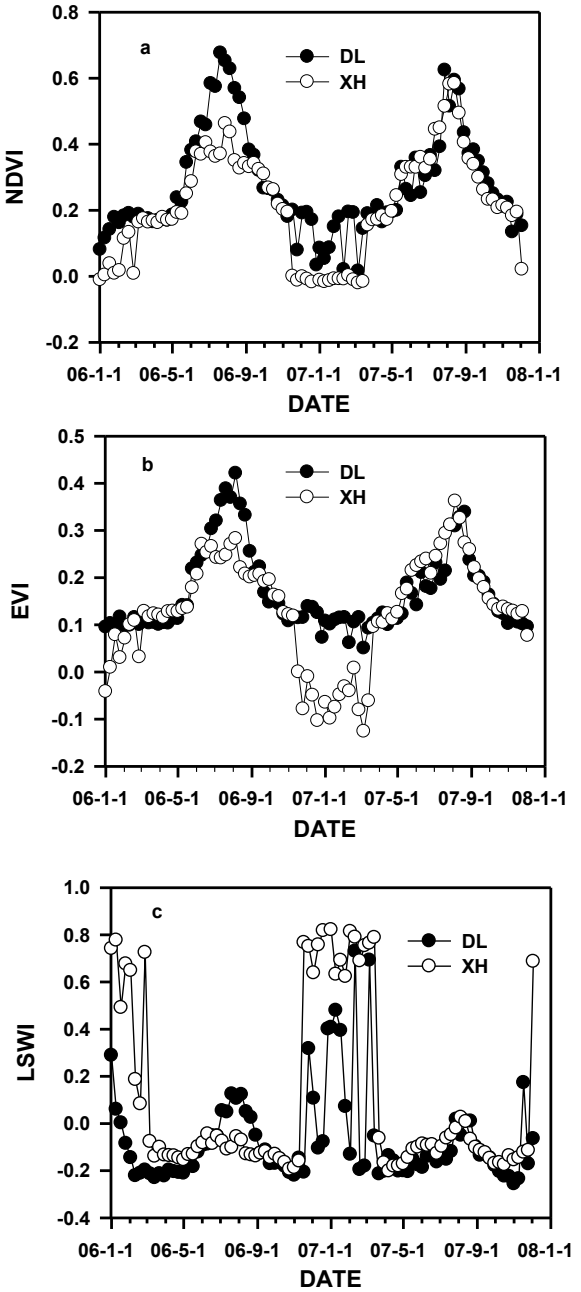

Fig. 3 Seasonal dynamics of *NDVI* (a), *EVI* (b) and *LSWI* (c) during the growing season in 2006-2007 for the two steppes.

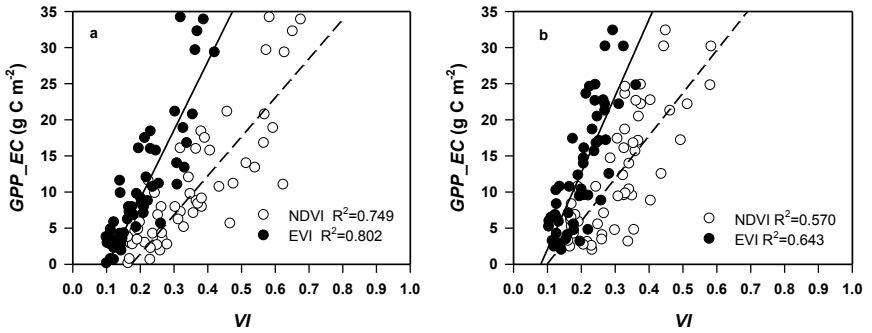

Fig.4 Simple linear regression analysis between GPP and vegetation indices (dash line: *NDVI*; solid line *EVI*) in DL (a) and XH (b)

3.3. Evaluation VPM predicted GPP

The VPM model was run at 8-daytime scale using the site-specific data of air temperature, *PAR* and vegetation indices in 2006 and 2007 for the two steppes. The seasonal dynamics of predicted *GPP* with the VPM model (*GPP_VPM*) was agreed well with the observed *GPP* with eddy covariance measurements (*GPP_EC*), but there still exist some discrepancies between *GPP_VPM* and *GPP_EC* (Fig.5). For example, several *GPP_VPM* values were lower than *GPP_EC* at the beginning or middle of the growing season. The simple linear regression model shows a good agreement between *GPP_VPM* and *GPP_EC* during the growing season in 2006 and 2007 for the steppes (Fig.6). The determination coefficient (R^2) of *GPP_VPM* with *GPP_EC* was 0.86 and 0.79 in 2006, 0.66 and 0.76 in 2007 for DL and XH, respectively. The relative errors (*RE*) of the two steppes were within the range of ±11 %, as for DL, the value was 7.9% and -10.4% in 2006 and 2007; for XH was -3.8% and 0.8%.The index of agreement (*IA*) also show a good agreement between *GPP_VPM* and *GPP_EC*, as the value of *IA* for XH is 0.94 in 2006 and 0.93 in 2007, 0.95 and 0.92 for DL, respectively.

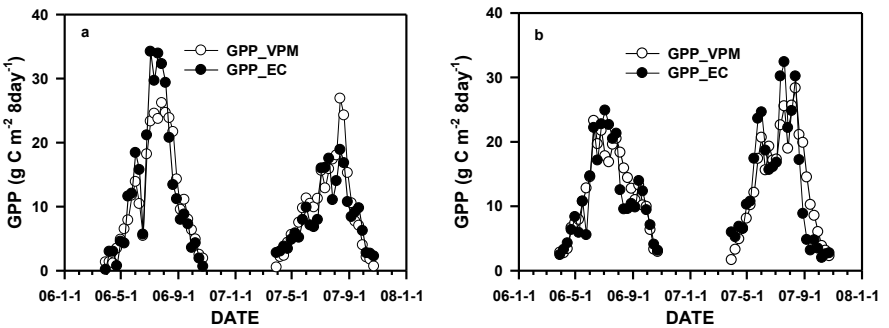

Fig.5 Comparison of the seasonal dynamics between the observed *GPP* (*GPP_EC*) and predicted *GPP* (*GPP_VPM*) in 2006 and 2007 for DL (a) and XH (b).

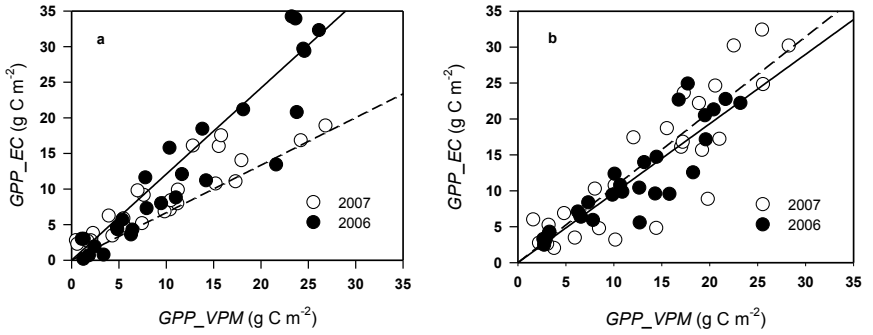

Fig.6 Simple linear regression analysis between the observed *GPP* (*GPP_EC*) and predicted *GPP* (*GPP_VPM*) in 2006 and 2007 for DL (a; 2006: y=1.129x, R^2=0.86, P<0.001; 2007: y=0.812x, R^2=0.66, P<0.001) and XH (b; 2006: y=0.964x, R^2=0.79, P<0.001; 2007: y=1.018x, R^2=0.76, P<0.001).

4. Discussion and Conclusion

In this study, the satellite-based VPM model was applied to two steppes of North China, and the predicted results compared with flux tower-based *GPP* values. For the study areas, previous studies have indicated that primary production is strongly controlled by the precipitation during the growing season, especially soil water content [28]. XH did not suffer manifest drought during the growing season in 2006 and 2007, when comparing the precipitation amount of the studying period with mean annual precipitation. But for DL, 2007 was the drier with only 52% of the long-term mean annual precipitation, whereas 2006 had close-to-normal precipitation (~112% of the long-term mean annual precipitation) [29]. This was the major reason for GPP during the growing season in 2007 fall behind that of 2006, as only taken up to 67.9% of the latter.

The simulation results of the VPM model have shown that the predicted *GPP* agreed well with the observed *GPP* of the two typical steppes in North China. The results from this study and earlier VPM studies of grassland [3, 13-15] indirectly support the Chlorophyll-FPARchl-EVI hypotheses and leaf water-LSWI hypothesis implemented in the VPM model. *FPAR* is a key biological property for estimating canopy photosynthesis [30, 31] because it characterizes vegetation canopy function and energy absorption capacity [32, 33]. Based on biochemical properties, the *FPAR* of vegetation canopy ($FPAR_{canopy}$) can be conceptually partitioned into the fraction of PAR absorbed by chlorophyll ($FPAR_{chl}$) and non-photosynthetic vegetation components (*FPARnpv*) [8, 34]. It has been found that FPARcanopy relates closely to *NDVI* [35, 36], and $FPAR_{chl}$ to *EVI* [8, 34, 36]. Wu *et al*. [12] also found that the *NDVI* was sensitive to greenness, and the *EVI* was more responsive to canopy structural variations, including chlorophyll and plant phenology. So utilizing the *EVI* to act as *FPAR* estimates greatly contributed to the accuracy of the model for *GPP* prediction.

Another important parameter in VPM model is the *LSWI*. In some previous studies, it has been found useful as an indicator of canopy water stress in the semiarid environment [37]. However, Sjöström *et al*. [38] found that the use of *LSWI* (=*SIWSI*) as a predictor of water stress in satellite data-driven primary production modeling in semi-arid ecosystems is limited when the fraction of vegetation apparently is too low for the index to provide accurate information on canopy water content. In this study, for the drier year in 2007 of DL, the predicted *GPP* by *VPM* generated the largest relative error, which may be partly due to the *LSWI* which has not been sufficient to reflect the water status, as found in Liu *et al* [15].

In summary, we have used flux data of two steppes in 2006-2007 in Inner Mongolia Plateau to estimate parameters of the VPM model and simulated the seasonal dynamics of *GPP* by integrating climate data and MODIS vegetation indices with the VPM model. These results indicate that the seasonal dynamics of *GPP* predicted by the VPM model matched well with observed *GPP* by the flux towers. The predicted *GPP* values of the four total growing seasons agreed reasonably with the observed *GPP* during the same period, with 5.7% mean relative error. The results also demonstrated that *EVI* had a stronger linear relationship with *GPP* than did *NDVI*. Additional studies are needed to validate the capability of the VPM model in arid or semi-arid ecosystems, especially suffering critical drought, and to develop more sensitive vegetation indices to reflect canopy or soil water status.

References

[1] Hao Y, Wang Y, Mei X, Huang X, Cui X, Zhou X, Niu H. CO_2, H_2O and energy exchange of an Inner Mongolia steppe ecosystem during a dry and wet year. *Acta Oecol* 2008; **33**: 133–43.

[2] Chen Z. Topography and climate of Xilin River Basin. In: the Chinese Academy of Sciences Eds. *Inner Mongolia Grassland Ecosystem Research Station*. Research on Grassland Ecosystem (No. 3), Beijing: Science Press; 1988, p. 13–22.

[3] Li Z, Yu G, Xiao X, Li Y, Zhao X, Ren C, Zhang L, Fu Y. Modeling gross primary production of alpine ecosystems in the Qinghai-Tibet Plateau using MODIS images and climate data. *Remote Sens Environ*, 2007; **107**: 510─9.

[4] Xiao JF, Zhuang QL, Baldocchi DD, Law BE, Richardson A D, Chen J, Oren R, Starr G, Noormets A, Ma S, Verma SB, Wharton S, Wofsy SC, Bolstad PV, Burns SP, Cook DR, Curtis PS, Drake BG, Falk M, Fischer ML, Foster DR, Gu L, Hadley JL, Hollinger DY, Katul GG, Litvak M, Martin T, Matamala R, McNulty S, Meyers TP, Monson RK, Munger JW, Oechel WC, Paw UKT, Schmid HP, Scott RL, Sun G, Suyker AE, Torn MS. Estimation of net ecosystem carbon exchange for the conterminous United States by combining MODIS and Ameriflux data. *Agric Forest Meteor* 2008;**148**: 1827─47.

[5] Running SW, Nemani RR, Heinsch FA, Zhao MS, Reeves M, Hashimoto H. A continuous satellite-derived measure of global terrestrial primary production. *Bioscience* 2004; **54**: 547─60.

[6] Turner DP, Ritts WD, Cohen WB, Maeirsperger TK, Gower ST, Kirschbaum AA, Running SW, Zhao M, Wofsy SC, Dunn AL, Law BE, Campbell JL, Oechel WC, Kwon HJ, Meyers TP, Small EE, Kurc SA, Gamon JA. Site-level evaluation of satellite-based global terrestrial gross primary production and net primary production monitoring. *Glob Change Biol* 2005; **11**: 666─84.

[7] Garbulsky M F, Penuelas J, Papale D, Filella I. Remote estimation of carbon dioxide uptake by a Mediterranean forest. *Glob Change Biol* 2008; **14**: 2860─7.

[8] Xiao XM, Hollinger D, Aber J, Goltz M, Davidson EA, Zhang Q. Satellite-based modeling of gross primary production in an evergreen needle-leaf forest. *Remote Sens Environ* 2004; **89**: 519─34.

[9] Xiao XM, Zhang QY, Braswell B, Urbanski S, Boles S, Wofsy S, Berrien M, Dennis O. Modeling gross primary production of temperate deciduous broadleaf forest using satellite images and climate data. *Remote Sens Environ* 2004; **91**: 256─70.

[10] Xiao XM, Zhang QY, Hollinger D, Aber J, Moore B. Modeling gross primary production of an evergreen needle-leaf forest using MODIS and climate data. *Ecol Appl* 2005; **15**: 954─69.

[11] Xiao XM, Zhang QY, Saleska S, Hutyra L, Camargo PD, Wofsy S, Frolking S, Boles S, Keller M, Moore B. Satellite-based modeling of gross primary production in a seasonally moist tropical evergreen forest. *Remote Sens Environ* 2005; **94**: 105─22.

[12] Wu JB, Xiao XM, Guan DX, Shi TT, Jin CJ, Han SJ. Estimation of the gross primary production of an old-growth temperate mixed forest using eddy covariance and remote sensing. *Int J Remote Sens* 2009; **30**: 463─79.

[13] Wu WX, Wang SQ, Xiao XM, Yu GR, Fu YL, Hao YB. Modeling gross primary production of a temperate grassland ecosystem in Inner Mongolia, China, using MODIS imagery and climate data. *Sci China Ser D* 2008; **51**: 1501─12.

[14] Wang HS, Jia GS, Feng JM, Zhao TB, and Ma ZG. Modeling gross primary production by integrating satellite data and coordinated flux measurements in arid and semi-arid China. *Atmos Ocean Sci Lett* 2010; **1**:7─13.

[15] Liu J, Sun OJ, Jin H, Zhou Z and Han X. Application of two remote sensing GPP algorithms at a semiarid grassland site

of North China. *J Plant Ecol* 2011; doi:10.1093/jpe/rtr019.

[16] Yan H, Fu Y, Xiao X, Huang HQ, He H, Ediger L. Modeling gross primary productivity for winter wheat-maize double cropping system using MODIS time series and CO_2 eddy flux tower data. *Agr Ecosyst Environ* 2009; **129**: 391–400.

[17] Chen S, Chen J, Lin G, Zhang W, Miao H, Wei L, Huang J, Han X. Energy balance and partition in Inner Mongolia steppe ecosystems with different land use types. *Agr Forest Meteorol* 2009; **149**: 1800–9.

[18] Wang JW, Cai YC. Studies on genesis, types and characteristics of the soils of the Xilin River Basin. In: the Chinese Academy of Sciences Eds, *Inner Mongolia Grassland Ecosystem Research Station. Research on Grassland Ecosystem* (No. 3) Beijing: Science Press; 1988. p. 23–83.

[19] Lu N, Chen S, Wilske B, Sun G and Chen J. Evapotranspiration and soil water relationships in a range of disturbed and undisturbed ecosystems in the semi-arid Inner Mongolia, China. *J Plant Ecol* 2011; **4**:49–60.

[20] Webb EK, Pearman GI, Leuning R. Correction of flux measurements for density effects due to heat and water vapour transfer. *Q J Roy Meteor Soc* 1980; **106**: 85–100.

[21] Wilczak JM, Oncley SP, Stage SA. Sonic anemometer tilt correction algorithms. *Bound-Layer Meteorol* 2001; **99**: 127–50.

[22] Falge E, Baldocchi D, Olson R, Anthonic P, Aubinetd M, Bernhofere C, Burba G, Ceulemans R, Clement R, Dolman H, Granier A, Gross P, Grünwald T, Hollinger D, Jensen N, Katul G, Keronen P, Kowalski A, Lai CT, Law BE, Meyers T, Moncrieff J, Moors E, Munger JW, Pilegaard K, Rannik Ü, Rebmann C, Suyker A, Tenhunen J, Tu K, Verma S, Vesala T, Wilson K, Wofsy S.Gap filling strategies for defensible annual sums of net ecosystem exchange. *Agric For Meteorol* 2001; **107**: 43–69.

[23] Tucker CJ. Red and photographic infrared linear combinations for monitoring vegetation. *Remote Sens Environ* 1979; **8**: 127–50.

[24] Huete AR, Liu HQ, Batchily K, Leeuwen W. A comparison of vegetation indices over a global set of TM images for EOS-MODIS. *Remote Sens Environ* 1997; **59**: 440–51.

[25] Raich JW, Rastetter EB, Melillo JM, Kicklighter DW, Steudler PA, Peterson BJ, Grace AL, Moore B, Vorosmarty CJ. Potential net primary productivity in South America: Application of a global model. *Ecol Appl* 1991; **1**: 399–429.

[26] Ahl DE, Gower ST, Mackay DS, Burrows SN, Norman JM and Diak GR. Heterogeneity of light use efficiency in a northern Wisconsin forest: implications for modeling net primary production with remote sensing. *Remote Sens Environ* 2004; **93**: 168–78.

[27] Willmott C J. Some comments on the evaluation of model performance. *Bull Am Meteorol Soc* 1982; **63**:1309–13.

[28] Li ZQ and Ren JZ. The models of suitability degree of grassland organism and their application. *Chinese Journal of Ecology*, 1997; **16**:71–5 (in Chinese).

[29] Zhang P, Chen S, Zhang W, Miao H, Chen J, Han X and Lin G. Biophysical regulations of NEE light response in a steppe and a cropland in Inner Mongolia. *J Plant Ecol*, 2011; doi:10.1093/jpe/rtr017.

[30] Goetz SJ, Prince SD, Goward SN, Thawley MM and Small J. Satellite remote sensing of primary production: an improved production efficiency modelling approach. *Ecol Model* 1999; **122**: 239–55.

[31] Seaquist JW, Olsson L, Ardo J. A remote sensing-based primary production model for grassland biomes. *Ecol Model* 2003; **169**: 131–55.

[32] Myneni R, Knyazikhin Y, Glassy J, Votava P, Shabanov N. User's guide fPAR, LAI (ESDT: MOD15A2) 8-day composite NASA MODIS land algorithm, Terra MODIS land team. 2003; http://cybele.bu.edu/modismisr/products/modis/userguide.pdf.

[33] Myneni RB, Hoffman S, Knyazikhin Y, Glassy J, Tian Y, Wang Y, Song X, Zhang Y, Smith GR, Lotsch A, Morisette JT, Votava P, Nemani RR, Running SW. Global products of vegetation leaf area and fraction absorbed PAR from year one of MODIS data. *Remote Sens Environ* 2002; **83**: 214–31.

[34] Zhang QY, Xiao XM, Braswell B, Linder E, Baret F, Moore B. Estimating light absorption by chlorophyll, leaf and canopy in a deciduous broadleaf forest using MODIS data and a radiative transfer model. *Remote Sens Environ* 2005; **99**: 357–71.

[35] Goward SN, Huemmrich KF.Vegetation canopy PAR absorptance and the normalized difference vegetation index –An assessment using the SAIL model. *Remote Sens Environ* 1992; **39**: 119–40.

[36] Zhang QY, Xiao XM, Braswell B, Linder E, Ollinger S, Smith ML, Jenkins JP, Baret F, Richardson AD, Moore B,

Minocha R. Characterization of seasonal variation of forest canopy in a temperate deciduous broadleaf forest, using daily MODIS data. *Remote Sens Environ* 2006; **105**: 189–203.

[37] Fensholt R and Sandholt I. Derivation of a shortwave infrared water stress index from MODIS near– and shortwave infrared data in a semiarid environment. *Remote Sens Environ* 2003; **87**: 111–21.

[38] Sjöström M, Ardö J, Eklundh L, ElTahir BA, ElKhidir HAM, Hellström M, Pilesjö P, Seaquist J. Evaluation of satellite based indices for gross primary production estimates in a sparse savanna in the Sudan. *Biogeosci* 2009; **6**: 129–38.